NONLINEAR EFFECTS IN RIGID POROUS LAYERS: MEASUREMENT AND MODELLING

O Umnova University of Hull, Hull, England, HU6 7RX
K Attenborough University of Hull, Hull, England, HU6 7RX
E Standley University of Hull, Hull, England, HU6 7RX
A Cummings University of Hull, Hull, England, HU6 7RX

1 INTRODUCTION

In porous materials the dominating nonlinearity is associated with the growth of flow resistivity with flow velocity. It leads to an excess sound attenuation inside the material which has been observed in highly porous fibrous materials and porous ceramics[1,2]. An equivalent fluid model of Johnson[3] with effective flow resistivity values dependent on Reynold's number was first employed to explain the nonlinear behaviour of rigid porous materials assuming constant flow through the sample[4]. Thermal effects were included by means of the complex compressibility function introduced by Champoux and Allard [5] and Lafarge [6]. The present paper offers a development of the "nonlinearisation "of the equivalent fluid model but allows for particle velocity variations within the sample. The resulting nonlinear model enables prediction of the acoustical properties of hard backed porous single and multiple porous layers at high intensities of incident sound.
In Section I A of this paper the model for nonlinear impedance and reflection coefficient of a single hard backed layer is described. As a result of this an analytical expression for the dependence of the reflection coefficient and surface impedance of a layer on the incident pressure amplitude is obtained.
In Section I B the model is extended to an arbitrary number of porous layers. The resulting system of nonlinear algebraic equations requires numerical solution to give the dependence of surface impedance and reflection coefficient on incident pressure amplitude.
In Section II, results are compared with data. Surface admittance and reflection coefficient of a single layer have been measured at different levels of continuous acoustic excitation for hard-backed layers of lead balls and porous concrete. Data are compared with the nonlinear model predictions at different frequencies, particularly those near the layer resonances.
The model for multiple porous layers has been tested on triple layers of lead shot with different particle sizes in each component layer.
The main results of the paper are summarized in Conclusions.

2 MODEL FOR SURFACE IMPEDANCE AND REFLECTION COEFFICIENT DEPENDENCE ON SOUND AMPLITUDE

2.1 Single hard backed rigid porous layer

By introducing the dimensionless complex tortuosity $\alpha(\omega)$ and complex compressibility $C(\omega)$ of the fluid contained in a rigid porous material, the equations for pressure *p* and particle velocity *v* variations in the plane sound wave of angular frequency ω can be written in the following form:

$$-i\omega\alpha(\omega)\rho_0 v = -\partial_x p, \qquad -i\omega\frac{C(\omega)}{\rho_0 c_0^{\,2}} p = -\partial_x v, \qquad (1)$$

here c_0 is the adiabatic sound speed and ρ_0 is the density of air .

The dynamic (complex) tortuosity $\alpha(\omega)$ is approximated by the following function [3]:

$$\alpha(\omega) = \alpha_\infty + \frac{\sigma\phi}{-i\omega\rho_0}\sqrt{1+(-i\omega)\frac{4\alpha_\infty{}^2\rho_0\eta}{\sigma^2\phi^2\Lambda^2}}, \qquad (2)$$

where α_∞ is the tortuosity, σ is the flow resistivity, Λ is the characteristic viscous length, ϕ is the volume porosity and η is the coefficient of dynamic viscosity for air. Similarly, the dynamic compressibility $C(\omega)$ is approximated by [5,6]:

$$C(\omega) = \gamma - (\gamma-1)\left(1+\frac{\eta\phi}{-i\omega\rho_0 k_0' N_{pr}}\sqrt{1+(-i\omega)\frac{\rho_0 4k_0'^2 N_{pr}}{\eta\Lambda'^2\phi^2}}\right)^{-1}, \qquad (3)$$

where γ is the adiabatic constant, N_{pr} is the Prandtl number, k_0' is the thermal permeability, and Λ' is the characteristic thermal length. The number of parameters necessary to model sound propagation in granular materials can be reduced by using a similarity relationship between complex density and complex compressibility functions [7].

It is assumed that flow resistivity grows linearly with the particle velocity amplitude in the sound wave:

$$\sigma = \sigma_0(1+\xi\phi|v|) \qquad (4)$$

where ξ is Forchheimer's nonlinearity parameter which can be measured in standard flow resistivity tests. The factor of porosity in equation (4) allows for the difference between the particle velocity in the pores and the flow velocity measured outside the material.

Expression (4) is substituted in (2) to get the velocity-dependent complex tortuosity $\alpha(\omega, v)$.

The solution of equations (1) with a velocity-dependent complex tortuosity $\alpha(\omega, v)$ is performed by the method of slow varying amplitudes. First the dispersion relation is found in linear approximation i.e.

$$k(\omega) = \frac{\omega}{c_0}\sqrt{\alpha(\omega)C(\omega)} \qquad (5).$$

Then a solution of nonlinear equations is sought in the form

$$v = v_+(x)e^{ik(\omega)x} + v_-(x)e^{-ik(\omega)x}, \qquad p = \frac{\rho_0 c_0{}^2}{i\omega C(\omega)}\partial_x v, \qquad (6)$$

where $v_\pm(x)$ are the slow varying amplitudes of particle velocity in the forward and backward propagating waves. Expressions (6) are now substituted into (1) and the second derivatives of $v_\pm(x)$ are neglected to give a pair of first order nonlinear differential equations describing spatial changes in $v_\pm$:

$$\frac{dv_\pm}{dx} = \mp M(\omega)\left(\sqrt{1+i\frac{\omega_c}{\omega}(1+\xi\phi|v|)^2} - \sqrt{1+i\frac{\omega_c}{\omega}}\right)v_\pm, \qquad (7)$$

where

$$M(\omega) = (1-i)\frac{\alpha_\infty\omega^2 C(\omega)}{c_0^2 k(\omega)}\frac{\delta(\omega)}{2\Lambda}, \quad \omega_c = \frac{\sigma_0{}^2\phi^2\Lambda^2}{4\alpha_\infty{}^2\rho_0\eta} \text{ and } \delta(\omega) = \sqrt{\frac{2\eta}{\omega\rho_0}} \text{ is the viscous layer}$$

thickness.

To determine the normalised surface impedance of the layer $Z = \frac{1}{\rho_0 c_0}\frac{p(0)}{\phi v(0)}$ equations (7) have to be solved with conditions of flux continuity and pressure continuity at the material surface

$$v_i + v_r = \frac{p_i - p_r}{\rho_0 c_0} = \phi v(0) = \phi\left(v_+(0) + v_-(0)\right), \quad (8)$$

$$p_i + p_r = p(0) = \rho_0 c_0 \sqrt{\frac{\alpha(\omega)}{C(\omega)}}\left(v_+(0) - v_-(0) + \frac{1}{ik(\omega)}\left(\frac{dv_+}{dx} + \frac{dv_-}{dx}\right)\Big|_{x=0}\right) \quad (9)$$

and the condition of zero particle velocity on an impervious hard backing:

$$v(d) = v_+(d)e^{ik(\omega)d} + v_-(d)e^{-ik(\omega)d} = 0, \quad (10)$$

where *d* is the porous layer thickness. The reflection coefficient follows from $R = \frac{v_r}{v_i} = \frac{1-Z}{1+Z}$.

The solution of equations (7) has been performed using the mean-field approximation [8]. This leads to the following relationships between the velocity amplitudes on both sides of the layer:

$$v_+(d) \approx v_+(0)\exp\left[-M(\omega)\left(\frac{1}{2}\sqrt{1+i\frac{\omega_c}{\omega}\left(1+\xi\phi|v(0)|\right)^2} + \sqrt{1+i\frac{\omega_c}{\omega}\left(1+\xi\phi|v(d)|\right)^2} - \sqrt{1+i\frac{\omega_c}{\omega}}\right)d\right],$$

$$v_-(d) = v_-(0)\frac{v_+(0)}{v_+(d)} \quad . \quad (11)$$

By combining this with boundary conditions (7)-(9) the following transcendental equation for the dependence of surface impedance on incident pressure amplitude has been obtained:

$$Z(\omega) = \frac{1}{\phi}\sqrt{\frac{\alpha(\omega)}{C(\omega)}}\left(1 - G\left(\frac{2|p_i|}{\phi|1+Z(\omega)|\rho_0 c_0}\right)\right)\coth\left(-ik(\omega)d\left(1 - \frac{1}{2}G\left(\frac{2|p_i|}{\phi|1+Z(\omega)|\rho_0 c_0}\right)\right)\right), \quad (12)$$

where $G(x) = \frac{M(\omega)}{ik(\omega)}\left(\sqrt{1+i\frac{\omega_c}{\omega}\left(1+\xi\phi x\right)^2} - \sqrt{1+i\frac{\omega_c}{\omega}}\right)$.

2.2 Multiple hard backed rigid porous layer

The schematic representation of the studied multilayered absorber is shown in Figure1.

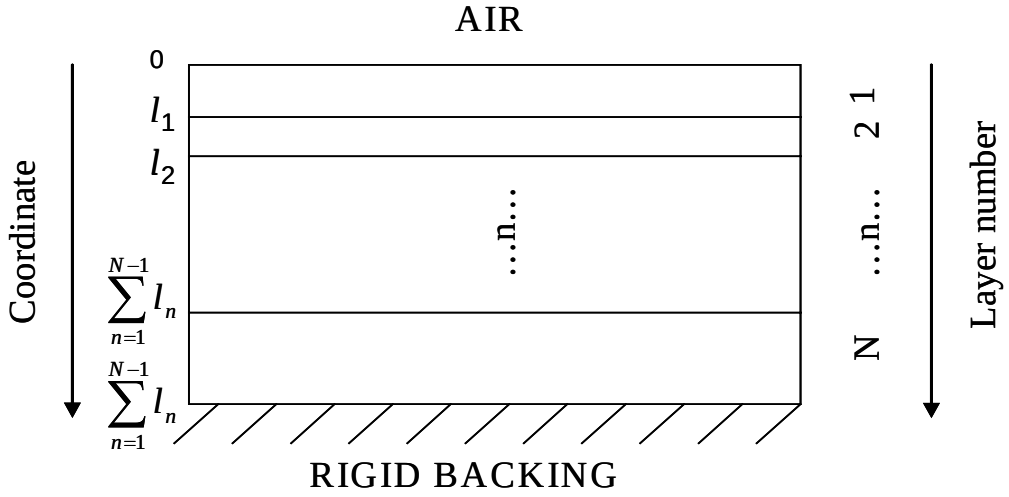

Figure 1. Schematic representation of multiple rigid layers

The equations for the pressure $p^{(n)}$ and particle velocity $v^{(n)}$ variations in the plane sound wave of angular frequency ω propagating in layer n (n=1…N, where N is the total number of layers) are

similar to (1) with $\alpha^{(n)}(\omega)$ and $C^{(n)}(\omega)$ being the complex density and complex compressibility respectively.

The complex tortuosity $\alpha^{(n)}(\omega)$ of the *n* -th layer is approximated using the equivalent fluid model again with following parameters: $\alpha_\infty{}^{(n)}$ is the tortuosity, $\sigma^{(n)}$ is the flow resistivity, $\Lambda^{(n)}$ is the characteristic viscous length, $\phi^{(n)}$ is the volume porosity of layer n material and η is the coefficient of dynamic viscosity for air. The complex compressibility function $C^{(n)}(\omega)$ is determined using the parameters $k_0{}'^{(n)}$ (thermal permeability), and $\Lambda'^{(n)}$ (characteristic thermal length in the *n*th layer.

It is assumed that the flow resistivity of the *n*th layer material grows linearly with particle velocity amplitude in the sound wave:

$$\sigma^{(n)} = \sigma_0{}^{(n)}\left(1+\xi^{(n)}\phi^{(n)}\left|v^{(n)}\right|\right)$$

where $\xi^{(n)}$ is the Forchheimer's nonlinearity parameter in the *n*th layer. The velocity dependent flow resistivity is substituted into the equivalent model expression for complex tortuosity in the same way as in Section 2 A.

Solution of the resulting nonlinear equation for each layer is sought in the form:

$$v^{(n)} = V_+{}^{(n)}(x) + V_-{}^{(n)}(x) = v_+{}^{(n)}(x)e^{ik^{(n)}(\omega)x} + v_-{}^{(n)}(x)e^{-ik^{(n)}(\omega)x}$$

$$p^{(n)} = \frac{\rho_0 c_0{}^2}{i\omega C^{(n)}(\omega)}\partial_x v^{(n)},$$

where $v_\pm{}^{(n)}$ are the slow varying amplitudes of particle velocity in the forward and backward propagating waves in the *n*th layer.

A pair of first order nonlinear differential equations similar to (7) describe spatial changes in $v_\pm{}^{(n)}$:

$$\frac{dv_\pm{}^{(n)}}{dx} = \mp M^{(n)}(\omega)\left(\sqrt{1+i\frac{\omega_c^{(n)}}{\omega}\left(1+\xi^{(n)}\phi^{(n)}\left|v^{(n)}\right|\right)^2} - \sqrt{1+i\frac{\omega_c^{(n)}}{\omega}}\right)v_\pm{}^{(n)}, \qquad (13)$$

where $M^{(n)}(\omega) = (1-i)\frac{\alpha_\infty{}^{(n)}\omega^2 C^{(n)}(\omega)}{c_0^2 k^{(n)}(\omega)}\frac{\delta(\omega)}{2\Lambda^{(n)}}$, $\omega_c{}^{(n)} = \left(\frac{\sigma_0{}^{(n)}\phi^{(n)}\Lambda^{(n)}}{2\alpha_\infty{}^{(n)}}\right)^2\frac{1}{\rho_0\eta}$.

In the following consideration velocities on each layer top and bottom are denoted as $V_\pm{}^{(n)}$ and $\tilde{V}_\pm{}^{(n)}$ respectively.

On the impervious hard backing, the boundary condition of zero velocity means that $\tilde{V}_+{}^{(N)} + \tilde{V}_-{}^{(N)} = 0$.

Another 2(N-1) equations result from the flux and pressure continuity at the boundaries between the layers:

$$\phi^{(m)}\left(V_+{}^{(m)} + V_-{}^{(m)}\right) = \phi^{(m-1)}\left(\tilde{V}_+{}^{(m-1)} + \tilde{V}_-{}^{(m-1)}\right), \qquad (14)$$

$$\frac{1}{C^{(m)}(\omega)}\left(\partial_x V_+{}^{(m)} + \partial_x V_-{}^{(m)}\right) = \frac{1}{C^{(m-1)}(\omega)}\left(\partial_x \tilde{V}_+{}^{(m-1)} + \partial_x \tilde{V}_-{}^{(m-1)}\right), \qquad (15)$$

where *m* = 2..N.

At the top layer boundary with air, the pressure and flux continuity equations can be written by introducing reflection coefficient *R* (defined previously):

$$\phi^{(1)}\left(V_+{}^{(1)} + V_-{}^{(1)}\right) = v_i + v_r = \frac{p_i}{\rho_0 c_0}(1+R), \qquad (16)$$

$$\frac{1}{C^{(1)}(\omega)}\left(\partial_x V_+^{(1)} + \partial_x V_-^{(1)}\right) = \frac{i\omega}{\rho_0 {c_0}^2} p_i(1-R). \quad (17)$$

The relationship between $V_\pm^{(n)}$ and $\tilde{V}_\pm^{(n)}$ can be found by approximate solution of (13) using mean field approximation and is defined by the following transcendental equation

$$\tilde{V}_\pm^{(n)} = V_\pm^{(n)} \exp\left(\pm s^{(n)}\left(\phi^{(n)}\left(V_+^{(n)} + V_-^{(n)}\right), \phi^{(n)}\left(\tilde{V}_+^{(n)} + \tilde{V}_-^{(n)}\right)\right) l^{(n)}\right), \quad (18)$$

where $s^{(n)}(a,b) = \dfrac{G^{(n)}(a) + G^{(n)}(b)}{2}$

$$G^{(n)}(a) = ik^{(n)} - M^{(n)}\left(\sqrt{1 + i\frac{\omega_c^{(n)}}{\omega}\left(1 + \xi^{(n)}|a|\right)^2} - \sqrt{1 + i\frac{\omega_c^{(n)}}{\omega}}\right)$$

and $l^{(n)}$ is layer number n thickness.

Further simplifications reduce (15) to a system of N+1 transcendental equations for the unknown functions $x_0 = (1+R),\ x_n = \dfrac{\phi^{(n)}\left(\tilde{V}_+^{(n)} + \tilde{V}_-^{(n)}\right)}{p_i}$:

$$x_0 A_1(p_i x_0, p_i x_1) + x_1 B_1(p_i x_0, p_i x_1) = 2,$$
$$x_{m-2} A_m(p_i x_{m-2}, p_i x_{m-1}) + x_{m-1} B_m(p_i x_{m-2}, p_i x_{m-1}, p_i x_m) + x_m C_m(p_i x_{m-1}, p_i x_m) = 0, \quad (19)$$
$$x_N = 0,$$

where

$$A_1(a,b) = -\frac{{c_0}^2 \rho_0 G^{(1)}(a)}{i\omega C^{(1)}(\omega)\phi^{(1)}} P^{(1)}(a,b) + 1,$$

$$B_1(a,b) = \frac{{c_0}^2 \rho_0 G^{(1)}(a)}{i\omega C^{(1)}(\omega)\phi^{(1)}} Q^{(1)}(a,b) \quad ,$$

$$A_m(a,b) = Q^{(m-1)}(a,b),$$

$$B_m(a,b,c) = \frac{G^{(m)}(b)}{G^{(m-1)}(b)} \frac{\phi^{(m-1)}}{\phi^{(m)}} \frac{C^{(m-1)}(\omega)}{C^{(m)}(\omega)} P^{(m)}(b,c) + P^{(m-1)}(a,b),$$

$$C_m(a,b) = -\frac{G^{(m)}(a)}{G^{(m-1)}(a)} \frac{\phi^{(m-1)}}{\phi^{(m)}} \frac{C^{(m-1)}(\omega)}{C^{(m)}(\omega)} Q^{(m)}(a,b).$$

$$P^{(n)}(a,b) = \frac{\exp\left(2s^{(n)}(a,b)l^{(n)}\right)+1}{\exp\left(2s^{(n)}(a,b)l^{(n)}\right)-1},$$

$$Q^{(n)}(a,b) = 2\frac{\exp\left(s^{(n)}(a,b)l^{(n)}\right)}{\exp\left(2s^{(n)}(a,b)l^{(n)}\right)-1},$$

Equations (19) have to be solved numerically to determine the reflection coefficient for multilayered absorber at different values p_i of the incident pressure amplitude.

3 COMPARISON WITH DATA

The main result from the model for single hard backed porous layer is that the reflection coefficient of the layer at resonance can experience either growth or decrease followed by subsequent growth

with incident pressure amplitude depending on the material parameters and layer thickness. Reflection coefficient measurements have been carried out on a layer of lead shot with 3.8mm particle diameter using a vertically installed impedance tube. A horizontal impedance tube has been used for similar measurements on a layer of porous concrete. Both materials show strong dependence of their flow resistivity on flow velocity (Figure 2 (a,b)).

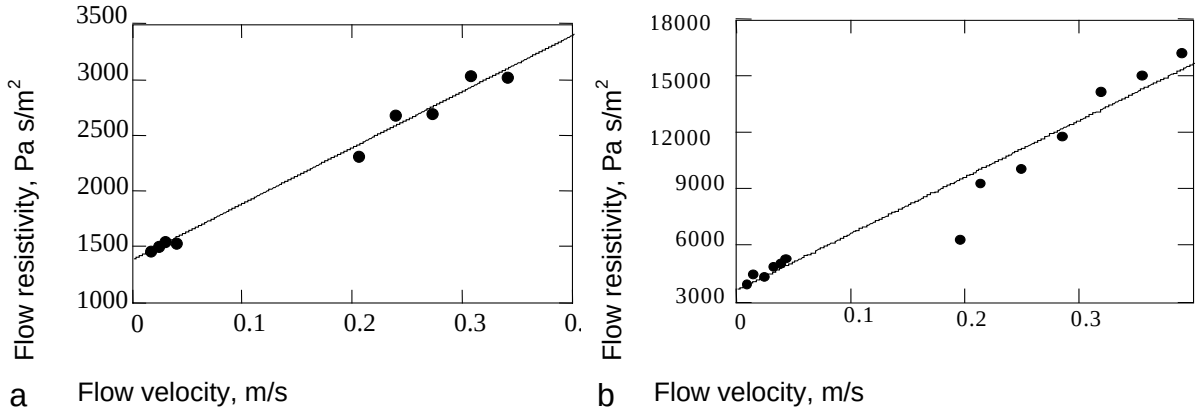

Figure 2. The dependence of flow resistivity on flow velocity and its straight line approximation, a- 3.8mm lead shot, b – porous concrete

The parameters of lead shot used in modelling have been either measured ($\phi = 0.385$, $\sigma_0 = 1373 Pa \times s/m^2$, $\xi = 3.7 s/m$) or estimated using cell model [9] ($\Lambda = 5.5 \times 10^{-4} m$) and empirical formula [10] ($\alpha_\infty = 1.6$). The complex compressibility function was estimated assuming identical spherical particles [7]. The reflection coefficient at resonance changes non-monotonously, as the incident pressure amplitude grows, in agreement with model predictions. This is illustrated in Figure 3 (a,b)

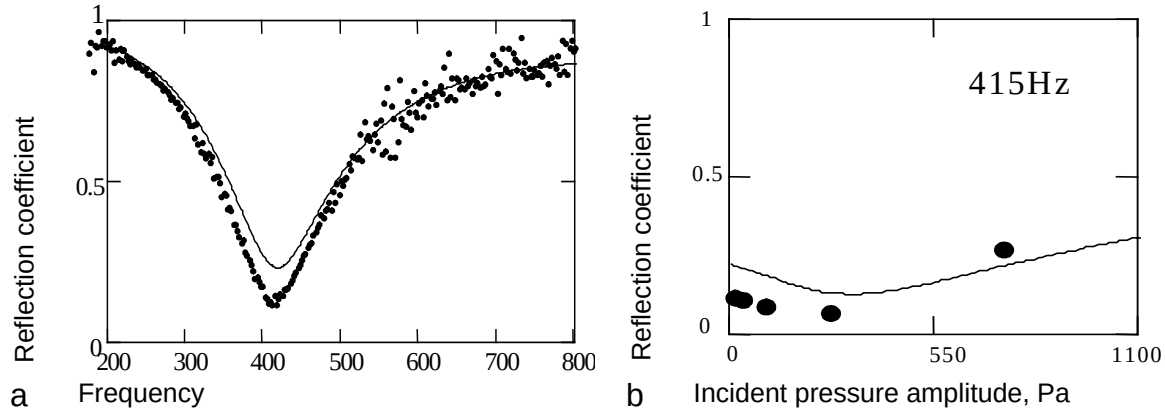

Figure 3. Predicted and measured behaviour of the reflection coefficient of a 10cm layer of lead shot (3.8mm particle diameter). A- Data (points) and Johnson/Allard/Lafarge model predictions (line) for frequency dependence at low amplitude sound (white noise). B – data and nonlinear model predictions for incident pressure amplitude dependence of the reflection coefficient at layer resonance (415Hz).

A different type of behaviour has been observed for a 10cm sample of porous concrete. The porosity, flow resistivity and Forchheimer's parameter of the material have been measured ($\phi = 0.3$, $\sigma_0 = 3619 Pa \times s/m^2$, $\xi = 8.3 s/m$). Other parameters have been adjusted to fit low intensity (linear) data with equivalent fluid model predictions ($\Lambda = 2.2 \times 10^{-4} m$, $\alpha_\infty = 1.8$). Spherical particles have been assumed again to estimate complex compressibility function. In this

case the reflection coefficient at resonance (500Hz) grows with incident pressure amplitude, as shown in Figure 4 (a,b).

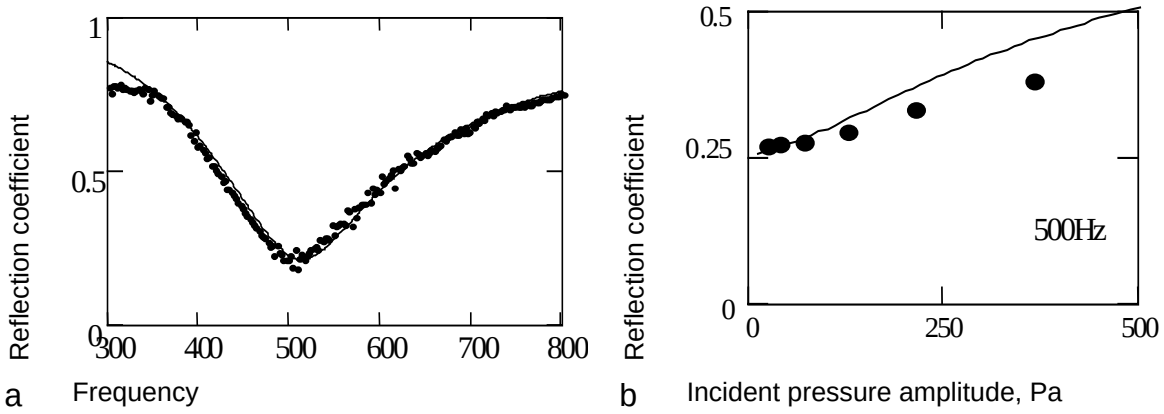

Figure 4. Predicted and measured behaviour of the reflection coefficient of a 10cm layer of porous concrete. A- Data and Johnson/Allard/Lafarge model predictions for frequency dependence at low amplitude sound (white noise). B – data and nonlinear model predictions for incident pressure amplitude dependence of the reflection coefficient at layer resonance (500Hz).

Experiments on multiple layers have been carried out on triple layers formed from lead shot with different particle sizes. The top layer was made from 3.8mm lead shot, 2.1mm lead shot was used for the intermediate layer ($\phi = 0.385$, $\sigma_0 = 3496 Pa \times s/m^2$, $\xi = 2.3 s/m$, $\Lambda = 2.8 \times 10^{-4} m$, $\alpha_\infty = 1.6$) and the smallest (1.25mm) size lead shot was used for the bottom layer ($\phi = 0.385$, $\sigma_0 = 6818 Pa \times s/m^2$, $\xi = 2 s/m$, $\Lambda = 2.1 \times 10^{-4} m$, $\alpha_\infty = 1.6$). The total thickness of the triple layers was always the same and equal to 14.7cm. The thicknesses of the individual layers have been changed (so that intermediate and bottom layers always had equal thicknesses) to study their influence on the overall absorption performance of the multiple layers. Three configurations with top layer thickness of 4.7cm, 7.7cm and 9.7 cm respectively have been studied. The resonant frequency for low intensity sound (395Hz, 405Hz and 410Hz respectively) changes only slightly with the first layer thickness. Both predicted and measured dependences of the reflection coefficient on the top layer thickness at different levels of incident sound of frequency 400Hz (close to resonance) are shown in Figure 5. For low amplitude sound the minimum reflection and consequently the highest absorption is obtained when the top layer thickness is close to 7.5cm. As the incident sound amplitude grows this configuration ceases to be the optimal one.

4 CONCLUSION

New models for predicting the impedance of single and multiple porous layers at high levels of incident sound have been presented. For a single layer it is predicted that, depending on the layer parameters, both growth and decrease followed by subsequent growth of the reflection coefficient at resonance can be observed when the amplitude of incident sound increases. This result has been confirmed by experiments with different types of rigid porous materials. It has been shown both theoretically and experimentally that multilayered porous absorbers designed to perform well at low intensity sound may not continue to have the optimum configuration as the sound level increases. The results suggest that both sound amplitude and the Forchheimer's nonlinearity of the material should be taken into account when estimating porous layer absorption properties.

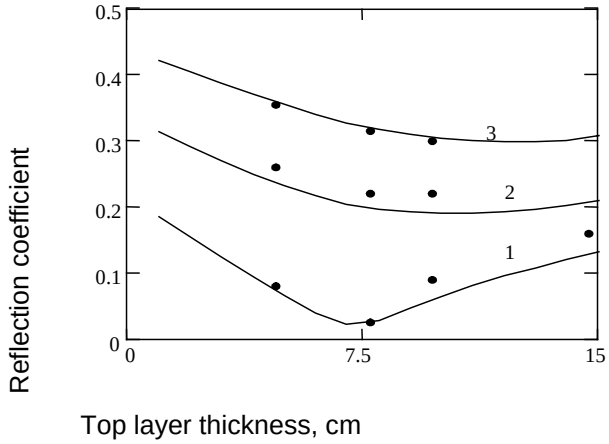

Figure 5. Reflection coefficient at 400Hz as a function of the top layer thickness l_1 at different levels of incident sound amplitudes ,$l_1+l_2+l_3$=14.7cm, $l_2=l_3$. Points – data, lines – predictions. 1 – low intensity sound (linear model), 2 – P_i=580Pa, 3 – P_i=1kPa

ACKNOWLEDGEMENT

The work is supported in part by USARSDG (UK), contract R7D 8901-EN-01 with funds from the US Army ERDC BT-25 Program.

5 REFERENCES

1 H.L.Kuntz, D.T.Blackstock,"Attenuation of intense sinusoidal waves in air-saturated, bulk porous materials", J.Acoust, Soc.Am., 81, 1723-1731, (1987).
2 J.D.McIntosh, R.F.Lambert, "Nonlinear wave propagation through rigid porous materials. Nonlinear parametrization and numerical solutions, II: Approximate analytical solutions", J.Acoust.Soc.Am, 88, 1939-1959, (1990).
3 D.L.Johnson, J.Koplik, R.Dashen, "Theory of dynamic permeability and tortuosity in fluid saturated porous media", J.Fluid.Mech., 176, 379-402, (1987).
4 Y.Auregan, M.Pachebat, "Measurement of the nonlinear behaviour of acoustical rigid porous materials", Phys.Fluids, 11, 1342-1345, (1999).
5 Y.Champoux, J.-F.Allard, "Dynamic tortuosity and bulk modulus in air – saturated porous media", J.Appl.Phys., 70, 1975-1979, (1991).
6 D.Lafarge, P.Lemariner, J.-F.Allard, V.Tarnow, "Dynamic compressibility of air in porous structures at audible frequencies", J.Acoust.Soc.Am., 102, 1995-2006, (1997).
7 O.Umnova, K.Attenborough, K.M.Li, "A cell model for the acoustical properties of packings of spheres", Acta Acustica, 87, 226-235, (2001).
8 H.M.Gibbs, Optical bistability, controlling light by light, Academic press, Orlando, 1985
9 O.Umnova, K.Attenborough, K.M.Li, "Cell model calculations of the dynamic drag parameters in packings of spheres", J.Acoust.Soc.Am., 107, 3113-3119, (2000).
10 K.Attenborough, "Models for the acoustical characteristics of air filled granular materials", Acta Acustica, 1, 213-226, (1993).